# High Content Screening in Zebrafish Speeds up Hazard Ranking of Transition Metal Oxide Nanoparticles

Sijie Lin,[†,∥] Yan Zhao,[‡] Tian Xia,[†,⊥,∥] Huan Meng,[†,⊥] Zhaoxia Ji,[†] Rong Liu,[†] Saji George,[†,⊥] Sijing Xiong,[†] Xiang Wang,[†] Haiyuan Zhang,[†] Suman Pokhrel,[¶] Lutz Mädler,[¶] Robert Damoiseaux,[†,§] Shuo Lin,[‡] and Andre E. Nel[†,⊥,∥,*]

[†]Center for Environmental Implications of Nanotechnology, [∥]Center for NanoBiology and Predictive Toxicology, and [§]Molecular Shared Screening Resources, California NanoSystems Institute, Los Angeles, California 90095, United States, [‡]Department of Molecular, Cell and Developmental Biology, and [⊥]Division of NanoMedicine, Department of Medicine, University of California, Los Angeles, California 90095, United States, and [¶]IWT Foundation Institute of Materials Science, Department of Production Engineering, University of Bremen, Germany

**ABSTRACT** Zebrafish is an aquatic organism that can be used for high content safety screening of engineered nanomaterials (ENMs). We demonstrate, for the first time, the use of high content bright-field and fluorescence-based imaging to compare the toxicological effect of transition metal oxide (CuO, ZnO, NiO, and $Co_3O_4$) nanoparticles in zebrafish embryos and larvae. High content bright-field imaging demonstrated potent and dose-dependent hatching interference in the embryos, with the exception of $Co_3O_4$ which was relatively inert. We propose that the hatching interference was due to the shedding of Cu and Ni ions, compromising the activity of the hatching enzyme, ZHE1, similar to what we previously proposed for $Zn^{2+}$. This hypothesis is based on the presence of metal-sensitive histidines in the catalytic center of this enzyme. Co-introduction of a metal ion chelator, diethylene triamine pentaacetic acid (DTPA), reversed the hatching interference of Cu, Zn, and Ni. While neither the embryos nor larvae demonstrated morphological abnormalities, high content fluorescence-based imaging demonstrated that CuO, ZnO, and NiO could induce increased expression of the heat shock protein 70:enhanced green fluorescence protein (*hsp70*:eGFP) in transgenic zebrafish larvae. Induction of this response by CuO required a higher nanoparticle dose than the amount leading to hatching interference. This response was also DTPA-sensitive. We demonstrate that high content imaging of embryo development, morphological abnormalities, and HSP70 expression can be used for hazard ranking and determining the dose–response relationships leading to ENM effects on the development of the zebrafish embryo.

**KEYWORDS:** high content imaging · transition metal oxide nanoparticle · dissolution · *hsp70* · zebrafish · hazard ranking

With thousands of different engineered nanomaterials (ENMs) being produced and included in consumer products, the inherent safety of these materials is of key importance for the acceptance and achievement of a sustainable technology to the benefits of humans and the environment.[1,2] While transition metal oxide nanoparticles are used with great success to improve the efficacy of catalysts, semiconductors, gas sensors, and sunscreens,[3−5] the possibility exists that materials such as ZnO, CuO, $Co_3O_4$, and NiO could pose biological hazard because of their ability to shed metal ions,[6] induce metabolic alkalosis,[7,8] or catalyze Fenton chemistry, leading to the generation of reactive oxygen species (ROS).[9,10] Since most efforts to assess the hazard of the transition metals have been carried out in cells, there is a paucity of data of their impact on intact organisms and animals in the environment. Animal screening is potentially costly, time-consuming, and often limits the number of animals that can be investigated in one experiment.

The development of a multiparametric high-throughput screening (HTS) assay that captures the sublethal and lethal effect of ENMs in mammalian cells is an example of how *in vitro* toxicological screening can be used to accelerate the pace of hazard assessment of the large number of new materials being developed.[11] While this tool has allowed us to perform *in vitro* hazard ranking and prioritizing animal experimentation, we also need to develop high content *in vivo* approaches to speed up ENM testing so as to be commensurate with the rate of expansion of nanotechnology.[12] Zebrafish, which has been used for modeling of biochemical and molecular disease mechanisms in humans, has proven to be a promising model for environmental risk assessment, including for toxicological assessment of ENMs, and presents an ideal opportunity for developing high-throughput approaches *in vivo*.[13−17] In a recent study, we demonstrated the utility of the zebrafish model to study hatching interference by dissolving ZnO nanoparticles, which are capable of inhibiting the hatching

* Address correspondence to anel@mednet.ucla.edu.

Received for review June 8, 2011 and accepted August 18, 2011.

**Published online August 18, 2011**
10.1021/nn202116p

enzyme, ZHE1, through Zn ion shedding.[18] Spherical and dendritic Ni nanoparticles have also been shown to exert hazardous effects in dechorionated zebrafish embryos through ion shedding as well as an independent contribution by particle shape.[19] Ag nanoparticles are highly toxic during zebrafish embryogenesis, including generation of several malformations and increased mortality.[20−23] In contrast, both mercaptobenzoic acid (MBA) and mercaptopyridine (MPY)-labeled Au nanoparticles are relatively safe and can be used as biocompatible imaging agents in the same organism.[24] However, during the toxicity evaluation of the aforementioned metal and metal oxides, the assessment is traditionally performed by visual examination of each embryo under a dissecting microscope, which is labor-intensive and limits the number of observations that can be made to obtain robust statistical results. Thus, advanced imaging technology and automated testing are key challenges toward developing high content screening of nanomaterials, chemicals, and drugs in zebrafish.[25]

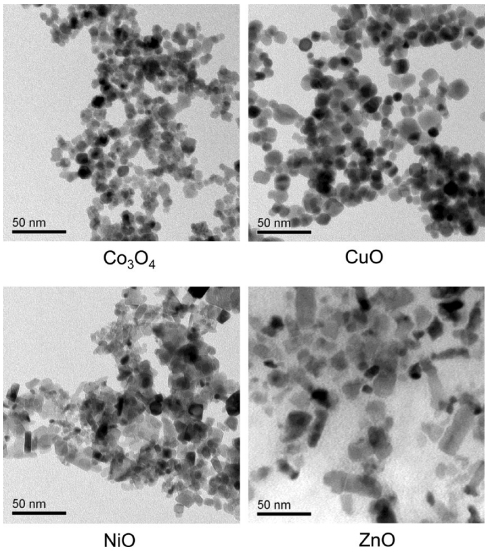


**Figure 1. Determination of the primary size of metal oxide nanoparticles. Representative TEM images of primary $Co_3O_4$, ZnO, NiO, and CuO nanoparticles ranging from 10 to 50 nm in diameter. The nanoparticles were dispersed by sonication in Holtfreter's medium supplemented with 100 ppm alginate. Aliquots of the particles suspended at 25 ppm were dried directly on the carbon-coated TEM grid prior to imaging. Images were captured at 80 kV accelerating voltage by TEM JEOL 1200 EX. The primary size of each particle was analyzed by NIH ImageJ software and listed in Table 1.**

Here, we demonstrate the establishment of two high content imaging platforms that can be used to screen for the toxicological effects of transition metal oxide nanoparticles in zebrafish embryos and early larvae. First, we will delineate the use of an imaging platform for bright-field imaging analysis, capable of capturing phenotypic and developmental abnormalities in embryos and larvae. For larvae, we will also describe a fluorescence-based approach to capture *hsp70*:eGFP expression in transgenic zebrafish. In order to apply these imaging tools to new ENMs not previously assessed, we utilized a series of transition metal oxide nanoparticles (CuO, NiO, and $Co_3O_4$) to compare to ZnO (positive control). Our results demonstrate profound interference in embryo hatching in parallel with *hsp70*:eGFP expression in larvae by CuO and NiO but not $Co_3O_4$. We show how high content image analysis can be used to perform hazard assessment in this organism in a time- and dose-dependent fashion. This approach can speed up the *in vivo* hazard assessment of ENMs and may allow the development of an automated system that can also be used for structure−activity analysis and hazard ranking.

## RESULTS

**Physicochemical Characterization of Transition Metal Oxide Nanoparticles.** A series of transition metal oxide nanoparticles representing adjacent elements in the periodic table (Co, Ni, Cu) were used to assess the impact on zebrafish embryos and larvae. ZnO was used as a positive control in these experiments.[26] These metal oxides are relevant from the perspective of their widespread use in industrial products and processes that could have an environmental footprint (Table S1 in the Supporting Information).[27] Moreover, the choice of these materials is interesting from the perspective of the differences in their rates of dissolution and ability to generate ROS based on lattice energies as well as band gap energy levels.[28] The primary sizes of the nanoparticles ranged from 20 to 50 nm, with some

**TABLE 1. Primary Size, Hydrodynamic Size, Polydispersity Index (PDI), and ζ-Potential of Transition Metal Oxide Nanoparticles**

| | | hydrodynamic size (nm)[b] | | ζ-potential (mV)[c] | |
|---|---|---|---|---|---|
| NPs | primary size (nm)[a] | without alginate | with alginate | without alginate | with alginate |
| $Co_3O_4$ | 12 ± 7 | 665 ± 46, 0.29 | 225 ± 28, 0.02 | −12.2 ± 0.97 | −26.35 ± 1.55 |
| CuO | 18 ± 5 | 617 ± 27, 0.29 | 284 ± 11, 0.07 | −11.9 ± 1.61 | −27.19 ± 2.91 |
| NiO | 40 ± 12 | 855 ± 37, 0.32 | 247 ± 17, 0.08 | −13.2 ± 1.70 | −28.76 ± 2.74 |
| ZnO | 23 ± 7 | 889 ± 32, 0.26 | 379 ± 2, 0.04 | −15.1 ± 2.10 | −29.66 ± 1.10 |

[a] Primary size of the particles in their dry state was obtained by transmission electron microscopy (JEOL, 1200 EX). [b] Hydrodynamic size was determined by high-throughput dynamic light scattering (HT-DLS, Dynapro Plate Reader, Wyatt Tech). [c] Particle ζ-potential was measured using ZetaPALS (Brookhaven Instruments, Holtsville, NY).

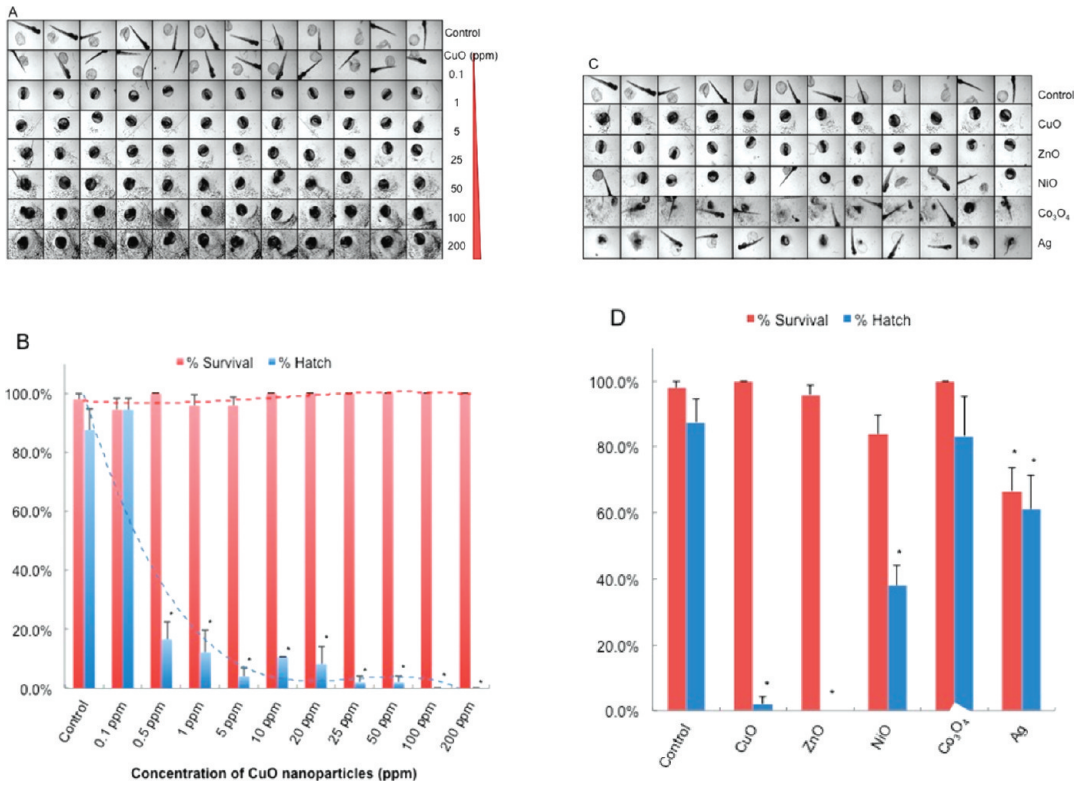


**Figure 2. Use of automated bright-field imaging (ImageXpress) for *in vivo* screening. (A) Representative image of a 96-well plate containing embryos viewed at 72 hpf in the presence of CuO nanoparticles. Each embryo was hand picked and placed in the well of a multiwell plate, which subsequently received 0.1−200 ppm CuO nanoparticles, starting at 4 hpf. Bright-field phase contrast images of each well were obtained through a 2× dry objective that autofocuses on each plate at 24 h intervals for five consecutive days. Each treatment group, including non-exposed controls, was assessed using 12 replicates. (B) Survival and hatching rates of embryos at 72 hpf clearly demonstrate hatching interference by CuO nanoparticles. Although the hatching interference was profound at doses ≥0.5 ppm, there was no apparent adverse effect on embryo survival, even at the highest CuO nanoparticle concentration (200 ppm). The statistical calculations are based on cumulative screening of 2000 embryos. Our high content capacity now enables us to screen 400 embryos every 72 h, amounting to 800 embryos per week. (C) Representative image of a 96-well plate comparing the screening of CuO, ZnO, NiO, $Co_3O_4$, and Ag nanoparticles (positive control) at 50 ppm. Parallel comparison across different nanoparticle types was accomplished using the same high content imaging technique. (D) Statistical analysis of embryos survival and hatching rates. Statistical significance was determined as $p < 0.05$ according to the student *t* test.**

agglomeration in their dry state as determined by transmission electron microscopy (TEM) (Figure 1). Extensive agglomeration occurred when the particles were dispersed in Holtfreter's medium, which was used to culture zebrafish embryos and larvae (Table 1). In order to improve particle dispersion and ability to perform hazard ranking with the stably suspended particles, the medium was supplemented with 100 ppm alginate, which represents an environmentally relevant capping agent known to stabilize ZnO nanoparticles.[18] Alginate reduced the hydrodynamic particle diameter to approximately 200−400 nm as determined by high-throughput dynamic light scattering (HT-DLS) (Table 1). Alginate supplementation also leads to a negative ζ-potential, ranging from −26 to −30 mV (Table 1).

**Use of Automated Bright-Field Phase Contrast Microscopy for High Content Imaging of Zebrafish Embryos.** Although the transparency and rapid development of zebrafish embryos facilitate the visual recognition and scoring of abnormalities under a dissection microscope, the necessity to do so in real time and to inspect each well on the plate is a labor-intensive task that could easily overlook subtle abnormalities as well as limiting the number of observations that can be made. Not only does this limit the statistical power of the observations but it also reduces the number of ENMs, material properties, and doses that can be assessed at one time. Due to these limitations, we implemented the use of an automated imaging device (ImageXpress) that is capable of collecting bright-field images at regular time intervals, allowing us to interpret and score the images at a time of our choosing. This system was implemented by placing single embryos into transparent U-bottom 96-well plates and then introducing the various nanoparticle dispersions at 4 h post-fertilization (hpf). The U-shaped well bottom allows embryo settling in a confined space that can be readily captured by rapid throughput imaging. Automated image collection was acquired through a 2× dry objective that autofocuses on each well of the plate every 24 h during a 5 day observation period. The automated image collection was then scored for phenotype characteristics such as

the success of embryo hatching, embryo mortality, and abnormal morphology of embryos and early larvae. Figure 2A shows the image analysis of a single plate which was viewed at 72 hpf following the exposure to 0.1−200 ppm CuO nanoparticles. Each concentration was assessed in 12 replicate wells, each containing one embryo. At least five replicate plates were used to obtain highly statistically significant data reflecting interference in embryo hatching, which starts at a dose as low as 0.5 ppm (Figure 2B). Interestingly, the nonhatched embryos exposed to CuO do not show any phenotypic malformations or evidence of mortality as may happen, for instance, in nano-Ag exposed embryos (Figure S1 in the Supporting Information).

The high content imaging platform was subsequently used to compare CuO to NiO and $Co_3O_4$ nanoparticles at doses of 0.5, 5, 25, 50, and 100 ppm. ZnO served as a positive control. This analysis demonstrated that while CuO, ZnO, and NiO exerted a significant effect on embryo hatching, starting at doses of 0.5, 5, and 50 ppm, respectively, $Co_3O_4$ had no effect even up to the highest dose. A comparative image-based analysis of these particles' effects as well as that of nano-Ag (comparative control) is shown in Figure 2C. Figure 2D shows a bar graph display of the data in addition to displaying the scoring of embryo mortality, which did not change with the exception of nano-Ag. Moreover, while nano-Ag induced pericardial edema and bent spines (Figure S1), no abnormal morphological features were identified in nonhatched embryos exposed to transition metal oxides. In order to exclude subtle abnormalities that may only manifest in the larvae after hatching, randomly selected embryos exposed for 48 h were anesthetized, dechorionated, and then imaged after embedding in low melting agarose. Images of both dorsal and ventral views confirmed the absence of minor morphological abnormalities, helping to confirm that the major impact of the metal oxides is on embryo hatching (Figure S2). This notion was further strengthened by dechorionating the embryos at 2 hpf and exposing them to a wide dose range of CuO for 4−48 hpf; most of the larvae developed normally without any phenotypic abnormalities (Figure S3).

**Metal Chelator, DTPA, Inhibits the Hatching Interference by the Metal Oxide Nanoparticles.** Particle dissolution and metal ion shedding are plausible mechanisms to explain the adverse effects of metal and metal oxide nanoparticles in zebrafish embryos.[29,30] In order to study this hypothesis, we assessed the dissolution rate of the transition metal oxide nanoparticles by inductively coupled plasma mass spectrometry (ICP-MS). These studies were carried out in Holtfreter's medium using identical tissue culture plates, medium volume, temperature, and incubation conditions as in the embryo exposure studies. Nanoparticles were placed in 96-well plates at 50 ppm and incubated at 28.5 °C for 1−48 h. The suspensions were removed, centrifuged, and the supernatants used to conduct ICP-MS, as described in Materials and Methods. While ZnO nanoparticles were clearly the most soluble, CuO and NiO released measurable amounts of the corresponding metals while $Co_3O_4$ showed little dissolution (Figure 3A). Holtfreter's medium contained negligible amounts of the measured transition metals (data not shown). In order to determine whether the free metal ions released from the particles could be responsible for hatching interference, we asked whether the inclusion of the metal ion chelator, diethylene triamine pentaacetic acid (DTPA), could exert an effect on the embryos. These experiments were carried out with 50 $\mu$M DTPA to stay below the threshold (100 $\mu$M) at which the chelator begins to affect the metalloproteinase activity of the hatching enzyme 1, ZHE1 (data not shown). Inclusion of DTPA at 4 hpf resulted in a dramatic reversal of the hatching interference of CuO, ZnO, and NiO, even at doses as high as 50 ppm (Figure 3B). The corresponding statistical analysis is shown in Figure 3C,D, which confirms that shedding of metal ions play a key role in hatching interference.

**Tracking the Presence of Free Metals in the Chorion.** The zebrafish chorion, composed of two major types of glycoproteins, acts as a barrier that protects the embryo against noxious physical and chemical stimuli.[31] While the natural pore size of the chorion ranges from 0.5 to 1 $\mu$m and is large enough to allow nanoparticle entry to the chorionic sac, we could not demonstrate the presence of particles in the chorionic fluid.[32,33] Instead, most of the particles that could be visualized were stuck to the surface of the chorion (data not shown). Similar results were obtained using 200 nm FITC-labeled $SiO_2$ nanoparticles which could not be visualized inside the chorionic sac.[34] However, one of the physiological functions of the chorion is to concentrate metal ions in the perivitelline fluid.[35,36] In order to determine whether transition metals shed by the metal oxide nanoparticles are indeed concentrated in the chorion, two metal-sensitive dyes, Newport Green DCF-K and Phen Green SK, were used to image the chorionic sac. Newport Green DCF-K emits green fluorescence when bound to $Zn^{2+}$, $Ni^{2+}$, and $Co^{2+}$, while $Fe^{3+}$, $Cu^{2+}$, and $Hg^{2+}$ act as quenchers of Phen Green SK's fluorescence.[37,38] Embryos exposed to 50 ppm CuO, ZnO, NiO, and $Co_3O_4$ for 24 h were rinsed with Holtfreter's and then microinjected with 2 nL of each dye at 50 $\mu$M. Figure 4A depicts the representative images of the Newport Green DCF-K injected embryos. This demonstrates that while the dye is insensitive to $Ca^{2+}$ and $Na^{+}$ in Holtfreter's medium, the addition of ZnO, NiO, and $Co_3O_4$ nanoparticles to these cultures could be seen to induce Newport Green fluorescence in the chorionic sac, while CuO was unable to do so. Moreover, inclusion of DTPA in the culture medium suppressed Newport Green

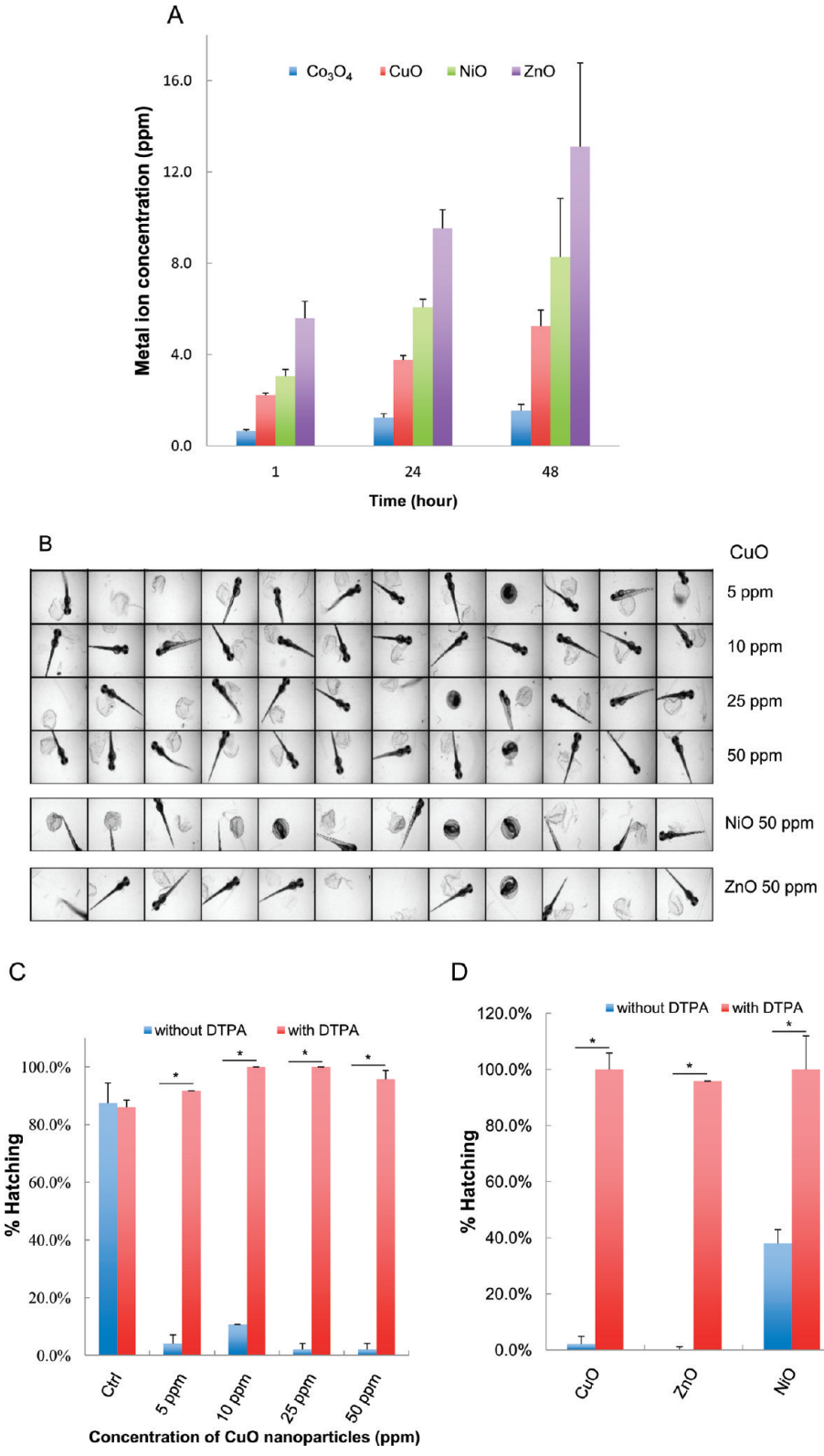


**Figure 3. Demonstration of the protective effect of the metal chelator, DTPA, on metal ion shedding and hatching interference. (A) Dissolution kinetics of each nanoparticle ($Co_3O_4$, CuO, NiO, and ZnO) in Holtfreter's medium. Triplicate nanoparticle suspensions at 50 ppm were placed in 96-well plates for 1−48 h at 28.5 °C. Supernatants of the dispersion were collected at 1, 24, and 48 h, and after nitric acid digestion, the corresponding metal ion (Co, Cu, Ni, and Zn) concentration was measured by ICP-MS. (B) Automated bright-field imaging at 72 hpf demonstrates the protective effect of DTPA on embryo hatching. CuO was used at 5, 10, 25, and 50 ppm, while NiO and ZnO were used at 50 ppm in the presence 50 $\mu$M DTPA. Embryo exposures commenced at 4 hpf and hatching interference was assessed at 72 hpf. (C) Scoring of the high content analysis of hatching interference by incremental doses of CuO nanoparticles. (D) Protective effect of DTPA was also observed in the embryos coexposed to 50 ppm NiO or 50 ppm ZnO.**

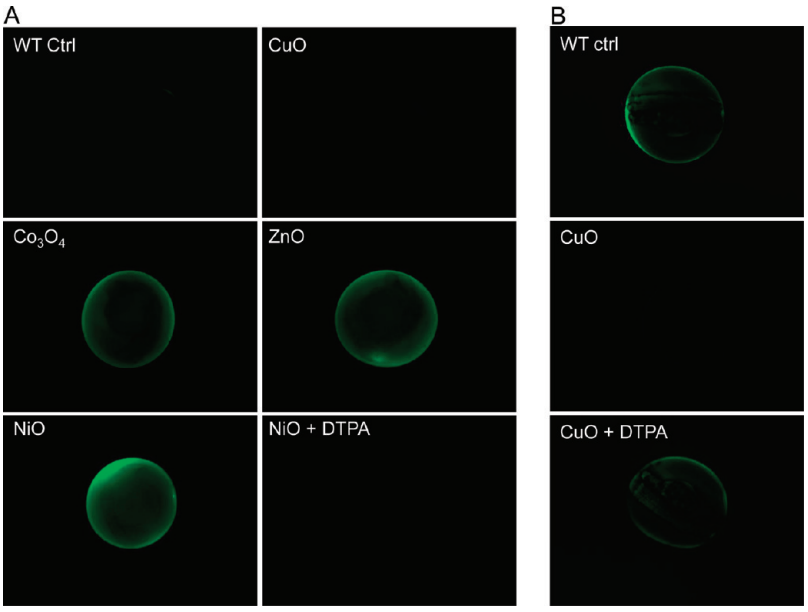


**Figure 4. Detection of free metals in the chorion. (A) Representative fluorescence images after microinjection of Newport Green DCF-K (50 $\mu$M) into the chorion. Embryos were exposed to 50 ppm nanoparticle dispersions at 4 hpf for 24 h. Embryos were washed with Holtfreter's medium and 2 nL of Newport Green DCF-K was microinjected into the chorion to detect the free metal ions. Fluorescence images were captured at the same filter sets (488/535 nm) and detection gain levels to allow quantitative comparison. Embryos exposed to the matching salt solutions ($ZnCl_2$ and $CuCl_2$ *etc.*) showed similar fluorescence patterns as the nanoparticles (data not shown). (B) Representative fluorescence images captured after microinjection of 50 $\mu$M Phen Green SK into the chorion. The fluorescence intensities of non-exposed embryo controls or to 50 ppm CuO in the absence or presence of DTPA are compared.**

**TABLE 2. Quantification of Metal Content by ICP-MS Analysis**

| | metal concentration (ppm) | | | |
|---|---|---|---|---|
| | 1 h exposure | | 24 h exposure | |
| NPs | inside chorion | outside chorion | inside chorion | outside chorion |
| $Co_3O_4$ | 0.320 ± 0.14 | 0.660 ± 0.10 | 2.130 ± 0.13 | 1.245 ± 0.33 |
| CuO | 0.85 ± 0.18 | 2.228 ± 0.16 | 9.900 ± 0.24 | 3.771 ± 0.37 |
| NiO | 0.715 ± 0.14 | 3.048 ± 0.60 | 11.300 ± 0.26 | 6.075 ± 0.70 |
| ZnO | 1.160 ± 0.20 | 5.600 ± 0.94 | 18.000 ± 0.47 | 9.525 ± 1.12 |

fluorescence in NiO-treated (Figure 4A) as well as ZnO and $Co_3O_4$-exposed embryos (data not shown). In contrast, Phen Green SK fluorescence was quenched by CuO exposure, but its fluorescence was restored in the presence of DTPA (Figure 4B). Quantification of the fluorescence intensity by NIH ImageJ software showed statistical significant changes in both the enhanced as well as quenched fluorescence intensities (Figure S4). Additional quantification of the metal uptake was provided by ICP-MS. Embryos exposed to nanoparticles for 1 and 24 h were washed and dried, following which chorionic fluid was collected by manually disrupting the chorion. The metal concentration in the chorionic fluid was compared to that in the medium, as demonstrated in Table 2. The data were also graphically displayed as the ratio of the metal concentration in the chorionic fluid *versus* the Holtfreter's medium, which demonstrated that compared to the ratios at 1 h, significant increases occur to achieve ratio values >1 by 24 h (Figure S5).

**Fluorescence-Based High Content Imaging To Show an Early Larval Stress Response.** While high content bright-field imaging provides rapid and clear evidence of hatching interference and the viability of the embryo, the absence of morphological abnormalities in the larvae does not exclude the possibility of more subtle toxicity. On the basis of the demonstration that $CdCl_2$ can activate eGFP expression in a transgenic zebrafish line (*hsp70*:eGFP), we asked whether this model could be used to demonstrate adverse effects at the larval stage.[39] Embryos derived from transgenic adult fish were plated in black-colored 96-well plates that contain a clear bottom to identify those with a transgene status based on eGFP expression in the lenses of the eyes by 24 hpf.[40] Following embryo hatching, the transgenic larvae were exposed to the metal oxide nanoparticles and then imaged using a high content imaging analysis system (Acumen) every 24 h for up to 72 h. A definitive increase in the green fluorescence intensity in the head region as well as the trunk and tail was observed in larvae exposed to 1 ppm $CdCl_2$ or heat-treated at 37 °C for 0.5 h (*i.e.*, the positive controls in Figure 5A). Moreover, larvae exposed to CuO and ZnO also resulted in an increase in GFP expression, while NiO and $Co_3O_4$ generated weak fluorescence signals (Figure 5A). Parallel real-time PCR was performed to quantitatively

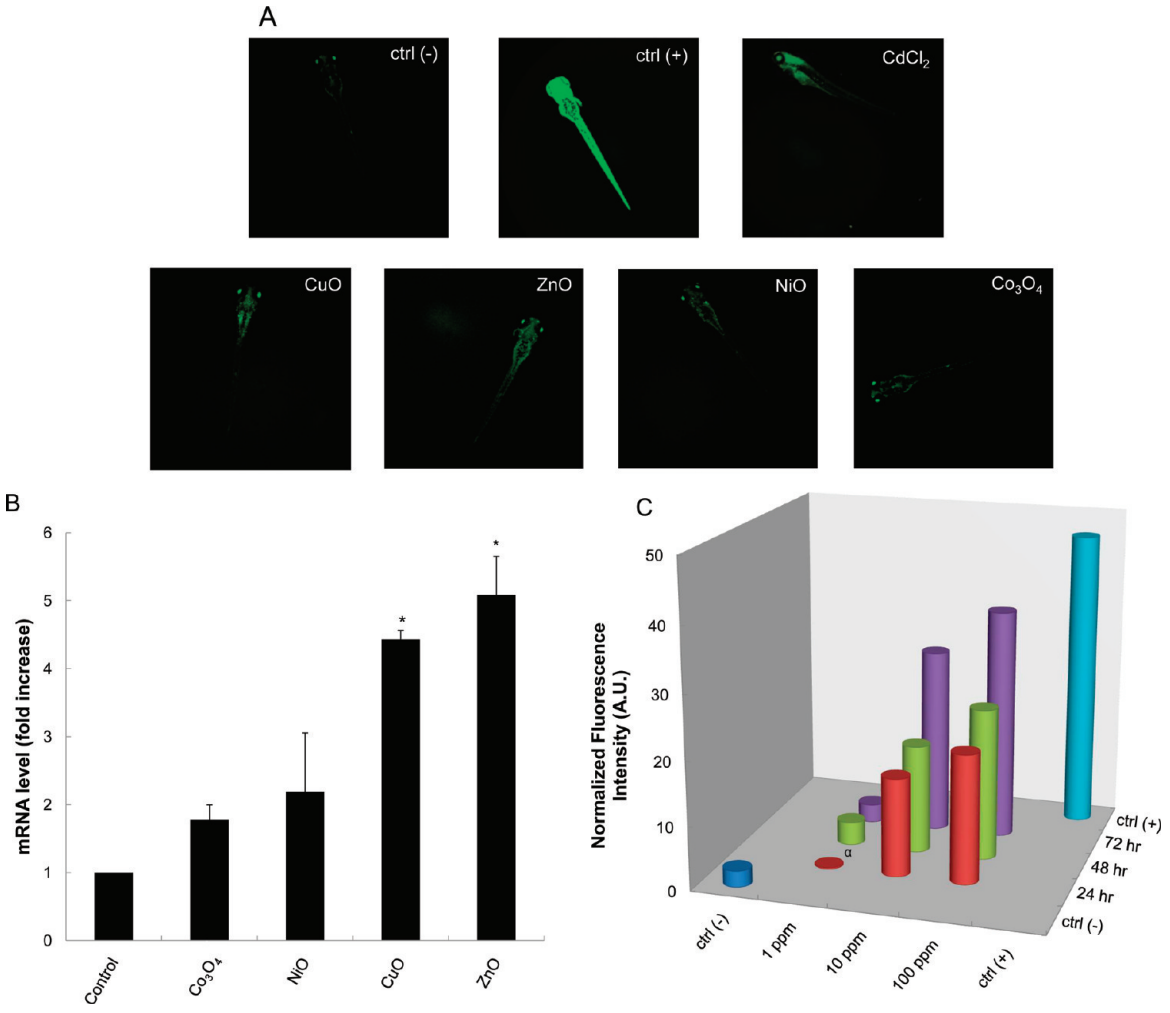


**Figure 5. Use of *hsp70*:eGFP transgenic zebrafish larvae for imaging of a protein unfolding stress response. (A) Representative fluorescence images of the early transgenic larvae captured by automated Acumen image analysis. The GFP-positive larvae were identified at 24 hpf based on fluorescence of the eye lenses. The exposure to nanoparticles commenced at 80 hpf and was carried for an additional 72 h. The fluorescence signals were collected at 535 nm with argon laser excitation at 488 nm. Heat-treated (37 °C, 0.5 h) or $CdCl_2$-exposed embryos (1 ppm) served as positive controls. The green fluorescence of the heat-treated larvae was ubiquitously distributed in all body tissues, while $CdCl_2$-induced fluorescence was seen mostly in the head region. Both CuO and ZnO exposed larvae had recognizable GFP expression, while NiO and $Co_3O_4$ resulted in weak GFP expression. (B) Similar trends were observed at the endogenous mRNA level. Assessment of *hsp70* mRNA expression in the nontransgenic larvae by RT-PCR shows a minimum of 4-fold increase during ZnO and CuO exposure, while the increase for NiO and $Co_3O_4$ was less than 2-fold. Statistical significance was determined as $p < 0.05$ according to the student *t* test. (C) eGFP expression of the transgenic larvae in response to increased CuO nanoparticle concentration and duration of exposure. This was accomplished by exposing the transgenic larvae to 1, 10, and 100 ppm CuO, starting at 80 hpf and collecting fluorescence images every 24 h for three consecutive days. The fluorescence intensity was scored by using NIH ImageJ software to obtain quantitative data. Statistical significance was achieved except for larvae exposed to 1 ppm of CuO at 24 hpf.**

assess endogenous *hsp70* mRNA expression in wild-type embryos exposed to the same particles. This confirmed that while *hsp70* transcription was significantly increased by CuO and ZnO, only a modest response could be observed in larvae exposed to NiO and $Co_3O_4$ (Figure 5B). More detailed analysis of CuO confirmed a dose- and time-dependent increase in the relative abundance of eGFP expression (Figure 5C). Please notice that although statistically significant eGFP expression could be achieved at 1 ppm by 48 h, robust expression required a dose of ≥10 ppm, which is at least an order of magnitude higher than the dose required for hatching interference (Figure 2B). Interestingly, the most affected body parts showing eGFP expression in response to CuO appeared in the surface layer of the head and tail regions, which differed from the ubiquitous fluorescence in the tissues of the heat-exposed larvae (Figure 6). Thus, while there is an agreement in the hierarchical effects of the different materials in terms of hatching interference and HSP70 expression, the embryos appear to be more sensitive than the hatched larvae.

## DISCUSSION

In this communication, we present two high content imaging platforms that were developed to screen

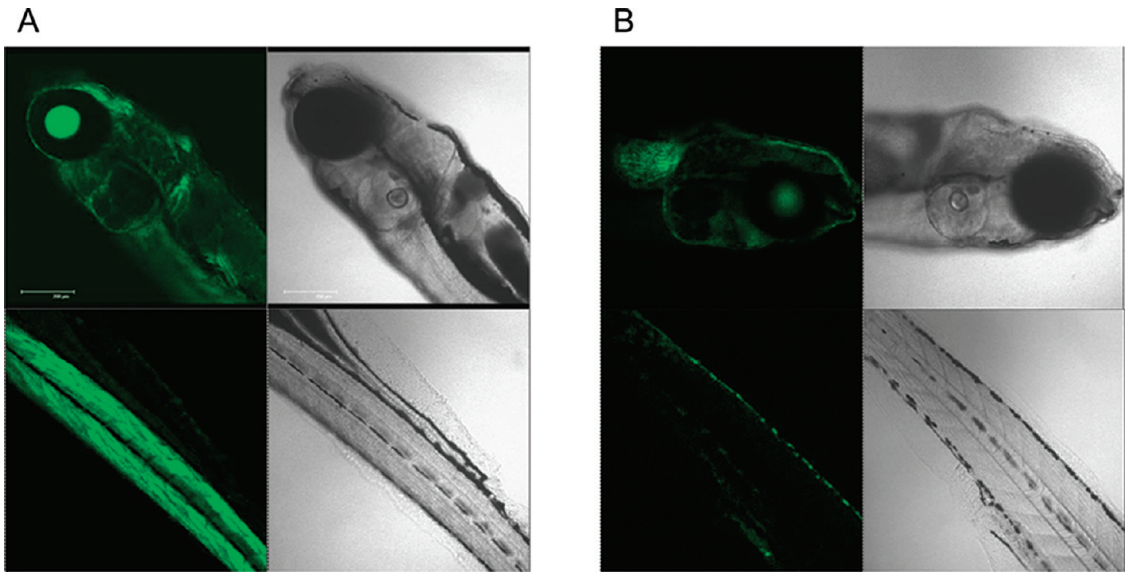


**Figure 6. Localization of GFP expression in the larval tissues by confocal microscopy. The representative confocal images of *hsp70*:eGFP transgenic zebrafish larvae treated by heat (37 °C, 0.5 h) (A) and CuO nanoparticles (10 ppm) (B). The green fluorescence was ubiquitously distributed in all tissue layers of heat-treated transgenic larvae. In contrast, only the surface layer of the head and tail region showed fluorescence increase in transgenic larvae exposed to CuO (10 ppm). All larvae were washed in Holtfreter's medium, anesthetized, and embedded in low melt agarose gel prior to confocal imaging (Leica SP1MP-Upright).**

transition metal oxide nanoparticles (CuO, NiO, and $Co_3O_4$) in zebrafish embryos and larvae. Following our previous demonstration using nano-ZnO (included as a positive control in this communication), we show that the high content imaging analysis by bright-field and fluorescent microscopy can be used to obtain dose- and time-dependent data for CuO and NiO adverse effects in the embryos and larvae. In contrast, $Co_3O_4$ had little effect on either response mode. Inclusion of the metal ion chelator, DTPA, in the exposure medium reversed both the hatching interference and induction of the heat shock response, thereby confirming the importance of metal shedding in the toxicological responses to these materials. These data were confirmed by ICP-MS analysis as well as the use of fluorescent dyes that detect metal ion uptake in the chorion. Thus, through the implementation of high content imaging, we demonstrate that it is possible to speed up hazard assessment in the zebrafish model.

Hatching interference of zebrafish embryos as a potential toxicological outcome has been demonstrated in our previous studies using ZnO nanoparticles.[18] However, similar analysis to assess other industrially relevant transition metal oxides has not been carried out previously in this animal model. Investigation of the environmental impact of CuO, NiO, and $Co_3O_4$ is relevant from an industrial perspective, where the use of these materials should be monitored for the possibility that they could land up in the environment (Table S1 in the Supporting Information).[27] Dissolution of the metal oxide particles with the potential to shed Cu, Ni, and Co ions is an important toxicological consideration as demonstrated by the use of ICP-MS as well as the reversal of hatching interference and the heat shock protein expression by the metal chelator, DTPA. As for most fish hatching enzyme, ZHE1 is a zinc metalloprotease.[41] Its crystal structure has recently been elucidated and exhibits an active center with a mitten shape into which the Zn ion is inserted.[41] This cleft contains three histidine residues that bind to Zn ion and possibly other transition metals of comparable atomic radius. Regarding the types of metal ions that can interact with histidine ligation sites, it has been proposed that there is a hierarchy of ion−ligand complexes, such that the affinity binding of Mn(II) < Fe(II) < Co(II) < Ni(II) < Cu(II) > Zn(II).[42] We propose that a similar hierarchy could also be involved in determining the interference of ZHE1 catalytic activity by transition metal oxides and that this could explain the different dose−response relationships of Cu, Zn, or Ni in the hatching embryo. The effective nanoparticle concentrations leading to hatching interference by CuO, ZnO, and NiO are 0.5, 5, and 50 ppm, respectively. Considering the dissolution rate of the individual nanoparticles (10.5 wt % for CuO, 26 wt % for ZnO, and 16.5 wt % for NiO over 48 h), the effective ion concentrations that could lead to hatching interference are estimated to amount to 0.05, 1.25, and 8 ppm for Cu, Zn, and Ni, respectively. We propose that the increased stability of the Cu/histidine ligand pair could explain the almost 2 orders of magnitude increase in its potency compared to nickel. This notion is further supported by a study showing that copper binding to histidine residues in a human prion protein is much higher than nickel.[43] To further investigate this hypothesis, we are in process of constructing recombinant ZHE1 protein to test the ion binding

constants and effect on enzymatic activity by different metal ions. If successful, recombinant ZHE1 could serve as a molecular tool to assist the screening of metal and metal oxide nanoparticles from an environment hazard perspective.

Larval assessment of HSP70 expression in transgenic zebrafish introduces an additional platform for high content screening of metal oxides. The heat shock protein family plays a critical role as chaperones for protein folding, translocation, and degradation and is relevant to the cellular stress response to heavy metals.[44] Heat shock factor (HSF), the transcription factor responsible for the activation of several heat shock gene promoters, is activated by elevated temperature, environmental stressors and toxicants, including heavy metals.[45,46] The best characterized heat shock protein is HSP70, a very sensitive stress-inducible member of this family that is often expressed in a tissue-specific fashion in a number of vertebrate species.[47,48] This is congruent with a significant increase in transgenic eGFP expression in response to ZnO and CuO in our study. Moreover, the transgene response was mirrored by expression of the endogenous *hsp70* gene, as determined by RT-PCR analysis. Interestingly, the tissues showing eGFP expression were mostly on the external larval surface, suggesting that skin uptake of the particles or metal ions may be responsible for this effect. Tissue-specific expression of the *hsp70*:eGFP gene has been demonstrated in the head and olfactory tissues of larvae exposed to Cd.[49] The increased dose requirements to generate a heat shock response compared to inhibition of embryo hatching suggests a higher threshold requirement for generation of adverse effects by Zn, Cu, and Ni in the larvae. It is also known that the zebrafish larvae with their more mature detoxification pathways are more resistant to toxic substances and hence may possess a higher level of tolerance to heavy metal ion concentrations.[50,51] The homologous regulation of gene responses in humans and the zebrafish opens the possibility to use additional transcriptional activation and cellular stress pathways to reconstitute additional high content screening approaches in transgenic zebrafish.

One of the main challenges for performance of *in vivo* ENM testing is the limitation in animal numbers that can be assessed in a single experiment. Thus, in order to achieve statistical significance, *in vivo* studies often have to involve repeat animal experiments, making these studies labor-intensive, time-consuming, and also raising ethical concerns. The implementation of a high-throughput approach in zebrafish accelerates ENM screening and also permits an increase of sample size, thereby strengthening the statistical power of the observations. Taking advantage of embryo transparency and the well-characterized developmental stages of the organism, bright-field imaging allows high content knowledge generation of the physicochemical properties of materials that pose a hazard at the *in vivo* level. Moreover, this approach allows high content *in vitro* screening to be compared to *in vivo* outcomes, as recently demonstrated by us.[11] The high volume data sets collected during high content imaging analysis could in the future also result in in-house development of software to perform automated *in silico* image analysis and hazard ranking. An example of the progress in this area is the ability to obtain embryo or larval images in each of the four different quadrants of the tissue culture wells and the ability to combine them into a single image (Figure S7). This overcomes the limited area (~4 × 3 mm) covered by the 2× dry objective, which occasionally fails to capture a complete image of swimming larvae or organisms that have grown too large in size (see Figure 2A,C). This software image analysis feature limits the chance of overlooking morphological abnormalities in the larvae. Coupled with robotic and automated embryo selection and transfer to tissue culture plates, we envisage that automated image analysis should soon achieve sufficient high-throughput capacity to assist *in vitro* ENM hazard assessment in the University of California Center for the Environmental Implications of Nanotechnology (UC CEIN) as well as the UCLA Center for NanoBiology and Predictive Toxicology.[52]

## CONCLUSION

We have successfully implemented high content imaging analysis to enhance our ability to screen the toxicological effects of ENMs in zebrafish embryos and early larvae. The profound hatching interference and stimulation of *hsp70* gene expression by CuO, ZnO, and NiO nanoparticles could be attributed to nanoparticle dissolution and shedding of transition metals. We were able to reverse these toxic effects with the metal ion chelator, DTPA. The establishment of a high content imaging platform will allow us to accelerate the screening and toxicity profiling of engineered nanoparticles.

## MATERIALS AND METHODS

**Materials and Reagents.** Nanoparticles ($Co_3O_4$, CuO, and ZnO) were synthesized in Dr. Mädler's laboratory by flame spray pyrolysis (FSP) as detailed by Teoh *et al.*[53] NiO was purchased from Sigma-Aldrich (CAS number: 1313-99-1). The metal ion sensitive dyes, Newport Green DCF-K and Phen Green SK, were purchased from Invitrogen (N-7990 and P-14313). Holtfreter's medium was prepared by dissolving NaCl (60 mM), $NaHCO_3$ (400 mM), KCl (0.6 mM), $MgSO_4$ (100 mM), and $CaCl_2$ (10 mM) in distilled water and adjusting the pH to 7.0.

**Physicochemical Characterizations of Transition Metal Oxide Nanoparticles.** CuO, ZnO, NiO, and $Co_3O_4$ nanoparticles, originally obtained in powder form, were dispersed in Holtfreter's medium supplemented with 100 ppm alginate by sonication to yield a stock solution of $5 \times 10^3$ ppm as previously described by us.[18] Physicochemical characterization of the dried particles was carried out by transmission electron microscopy (TEM), while particles suspended in Holtfreter's were used for high-throughput dynamic light scattering and measurement of the $\zeta$-potential. TEM samples were prepared by placing a drop of nanoparticle dispersion (25 ppm) on a carbon-coated TEM grid and waiting for the water to evaporate. Images were acquired at 80 kV accelerating voltage (JEOL 1200 EX), and the primary size was analyzed by NIH ImageJ software. The hydrodynamic size of the nanoparticles, dispersed in Holtfreter's medium, was determined by high-throughput dynamic light scattering (HT-DLS, Dynapro Plate Reader, Wyatt Technology) as described by Ji *et al.*[54] A ZetaPALS instrument (Brookhaven Instruments, Holtsville, NY) was used to measure the electrophoretic mobility of nanoparticles from which the $\zeta$-potential was derived by using Helmholtz−Smoluchowski equation.[55]

The dissolution kinetics of the nanoparticles in Holtfreter's medium was studied by inductively coupled plasma mass spectroscopy (ICP-MS). Two hundred microliters of a triplicate nanoparticle suspension was placed in the wells of a 96-well plate and kept at 28.5 °C under conditions similar to those used for zebrafish exposure. The particle dispersions were collected after 1, 24, and 48 h and centrifuged for 1 h at 20 000*g*. The supernatants were collected, and 50 $\mu$L aliquots from each supernatant were digested by 100% ultrahigh purity nitric acid for 3 h at 95 °C before drying and dissolving in 3 mL of 5% nitric acid. The metal ion concentrations (Cu, Zn, Ni, and Co) were measured by an Agilent 7500c quadrupole ICP-MS, and the dilution was taken into consideration to calculate original concentrations.

**Zebrafish Husbandry.** Wild-type and *hsp70*:eGFP transgenic zebrafish (*Danio rerio*) were housed and maintained in the UCLA zebrafish facility on a 14 L:10D photoperiod at 28.5 °C. The *hsp70*:eGFP line was constructed as described by Halloran *et al.*[56] Two pairs of male/female fish were placed in a single cage a day ahead of time and released in the next morning to trigger spawning. The embryos (2 hpf) were collected and rinsed with Holtfreter's solution to remove any residue on the embryo surface. The embryos were subsequently examined under a stereomicroscope (Zeiss, Stemi 2000) for viability and developmental stage before selection and nanoparticle exposure as described below. All procedures were carried out in accordance with the Animal Care and Use Committee guidelines at UCLA.

**Exposure of Zebrafish Embryos and Larvae to Nanoparticles.** Healthy embryos at the same developmental stage (2 hpf) were hand selected and placed one embryo per well in 96-well transparent, U-bottom plates. One hundred microliters of each nanoparticle suspension at working concentrations of 0.05, 0.5, 5, 25, 50, 100, and 200 ppm was added to the wells in the right at 4 hpf. To achieve robust statistical calculation, five replicate trials were carried out, each using 12 embryos. Observations of adverse biological outcomes, including hatching interference, phenotypic abnormalities and mortality (necrosis of the embryos), were carried out every 24 h for five consecutive days through the use of an automated bright-field imaging instrument (ImageXpress).

For the analysis of *hsp70*:eGFP expression, embryos harvested from the transgenic zebrafish (mixed heterozygous and homozygous) were placed in black multiwell plates that have transparent bottoms as described above and kept at 28.5 °C. The GFP-positive embryos were selected at 24 hpf on the basis of GFP expression in the lenses of the eyes. The hatched larvae (80 hpf) were exposed to nanoparticles at 80 hpf. Heat treatment at 37 °C for 0.5 h and exposure to 1 and 10 ppm $CdCl_2$ were used as positive controls for *hsp70*:eGFP expression. The fluorescence images were captured every 24 h after exposure for three consecutive days by automated fluorescence imaging (Acumen) as described below.

**High Content Imaging (ImageXpress and Acumen) and Data Analysis.** Microscope-based image analysis devices ImageXpress (Molecular Probes) and Acumen (Tip Labtech) were used to establish automated high content imaging. The multiwell plates containing the exposed embryos were placed on the fully automated stage of the ImageXpress, which provides 100 nm resolutions of the bright-field phase contrast images in the $x-y$ axis under a 2× dry objective. Transparent U-bottom multiwell plates were chosen to allow each embryo to be localized as close to the center as possible. For hatched embryos, 0.017% tricaine solution was used to anesthetize the larvae prior to imaging. Images were processed to score the hatch and mortality rates.

Fluorescence images of the transgenic early larvae were captured in each well by the automated fluorescence-based imaging device, Acumen. This instrument uses an argon laser (488 nm) to scan through the bottom of each well and collect fluorescence signals at 535 nm from each well simultaneously. The fluorescence intensities, which reflect the expression levels of the *hsp70*:eGFP gene, were further analyzed by Image J/NIH software.

**Enzymatic Embryo Dechorionation.** Groups of 1000 embryos were thoroughly washed and treated with 1 mg/mL Pronase solution to achieve chorion digestion within 5 min. The embryos were examined under a stereomicroscope (Zeiss, Stemi 2000) and Holtfreter's medium was added to terminate the digestion process, immediately following the dissociation of the first chorion. The embryos were washed several times to remove the detached chorions and placed into 96-well multiwell plates for nanoparticle exposure as described above.

**Analysis of Zebrafish *hsp70* Gene Expression in the Zebrafish by Real-Time PCR.** Real-time PCR was performed to examine the expression of *hsp70* gene in wild-type controls and embryos exposed to nanoparticles. A total of 50 embryos per group were collected at 72 and 152 hpf, respectively, and homogenized in 1 mL of TRIZOL reagent (Invitrogen). Subsequently, 2 $\mu$g of total RNA was reverse transcribed by Superscript III reverse transcriptase (Invitrogen). cDNA was amplified by real-time PCR using SYBR Green Supermix (BioRad), using the following primers: hsp70F 5′-tatctggggcagaaggtgac-3′, hsp70R 5′-ccgtcttcaatggtcaggat-3′. The gene expression levels were reported as fold-change (FC) relative to actin using the $\Delta\Delta Ct$ method where $FC = 2 - \Delta\Delta Ct$.[57]

**Phenotype Observation and Confocal Imaging.** Embryos exposed to the nanoparticles at 48 hpf were washed, anesthetized, and manually dechorionated by forceps before embedding in low melting agarose gel. This allowed for their positioning to obtain lateral and ventral views that can be used to detect phenotypic abnormalities. The confocal imaging of *hsp70*:eGFP transgenic larvae was conducted using a Leica SP1MP-Upright confocal microscope. Larvae exposed to nanoparticles were washed and anesthetized prior to imaging.

**Transition Metal Detection in the Chorion by Fluorescence Dyes and ICP-MS Analysis.** Transition-metal-sensitive fluorescent dyes, Newport Green DCF-K and Phen Green SK (Invitrogen), were dissolved in DMSO at 1 mM and diluted to a working concentration of 50 $\mu$M in Holtfreter's medium. Embryos exposed to 50 ppm nanoparticles (CuO, ZnO, NiO, and $Co_3O_4$) for 24 h were microinjected into the chorion with 2 nL of the dye solution into the chorion. The embryos were examined under a fluorescence microscope (Zeiss Observer D1). The increased fluorescence intensity (535 nm) of Newport Green DCF-K compared to controls was used as an indicator for uptake of transition metal ions in the chorion. Conversely, for Phen Green SK, the decrease in green fluorescence intensity was used as an indicator of the presence of metal ions capable of quenching the fluorescence.

ICP-MS analysis was used to further quantify the metal content in the chorionic fluid compared to the exposure medium. Embryos exposed to 25 ppm nanoparticles for 24 h were collected and washed in Holtfreter's medium. Excess water on the chorion was dried before breaking the chorion with fine forceps. The chorionic fluid collected from 20 embryos was centrifuged (20 000*g*, 1 h), and the supernatant was digested for ICP-MS analysis as described above. Simultaneously, we collected the exposure medium from each well and used the supernatant for ICP-MS analysis as described above.

*Acknowledgment.* This work is supported by the National Science Foundation and the Environmental Protection Agency

under Cooperative Agreement Number DBI 0830117. Any opinions, findings, conclusions or recommendations expressed herein are those of the author(s) and do not necessarily reflect the views of the National Science Foundation or the Environmental Protection Agency. This work has not been subjected to an EPA peer and policy review. Key support was provided by the U.S. Public Health Service Grants (RO1 CA133697, RO1 ES016746, RC2 ES018766, and U19 ES019528). We acknowledge Dr. Shane Que Hee, School of Public Health, University of California, Los Angeles, for the ICP-MS analysis. Fluorescence microscopy was performed at the CNSI Advanced Light Microscopy/Spectroscopy Shared Facility at UCLA.

*Supporting Information Available:* Additional table on the transition metal oxide nanoparticles production volume, application area and possible exposure routes and figures on detailed imaging of embryos, high content imaging of dechorionated embryos, fluorescence intensities analyses of microinjected metal ion sensitive dyes, quantification of metal content by ICP-MS, images obtained by fluorescence-based high content imaging, and four quadrant images obtained by bright-field high content imaging as described in the text. This material is available free of charge *via* the Internet at http://pubs.acs.org.

## REFERENCES AND NOTES


1. Gerber, C.; Lang, H. P. How the Doors to the Nanoworld Were Opened. *Nat. Nanotechnol.* **2006**, *1*, 3–5.
2. Scown, T. M.; van Aerle, R.; Tyler, C. R. Review: Do Engineered Nanoparticles Pose a Significant Threat to the Aquatic Environment? *Crit. Rev. Toxicol.* **2010**, *40*, 653–670.
3. Hsueh, T. J.; Hsu, C. L.; Chang, S. J.; Chen, I. Laterally Grown ZnO Nanowire Ethanol Gas Sensors. *Sens. Actuators, B* **2007**, *126*, 473–477.
4. Nel, A.; Xia, T.; Mädler, L.; Li, N. Toxic Potential of Materials at the Nanolevel. *Science* **2006**, *311*, 622–627.
5. Zhou, K.; Wang, R.; Xu, B.; Li, Y. Synthesis, Characterization and Catalytic Properties of CuO Nanocrystals with Various Shapes. *Nanotechnology* **2006**, *17*, 3939–3943.
6. Midander, K.; Cronholm, P.; Karlsson, H. L.; Elihn, K.; Möller, L.; Leygraf, C.; Wallinder, I. O. Surface Characteristics, Copper Release, and Toxicity of Nano- and Micrometer-Sized Copper and Copper (II) Oxide Particles: A Cross-Disciplinary Study. *Small* **2009**, *5*, 389–399.
7. Meng, H.; Chen, Z.; Xing, G.; Yuan, H.; Chen, C.; Zhao, F.; Zhang, C. Ultrahigh Reactivity Provokes Nanotoxicity: Explanation of Oral Toxicity of Nano-Copper Particles. *Toxicol. Lett.* **2007**, *175*, 102–110.
8. Chen, Z.; Meng, H.; Xing, G.; Chen, C.; Zhao, Y.; Jia, G.; Wang, T.; Yuan, H.; Ye, C.; Zhao, F. Acute Toxicological Effects of Copper Nanoparticles *in Vivo*. *Toxicol. Lett.* **2006**, *163*, 109–120.
9. Lee, D. H.; O'Connor, T. R.; Pfeifer, G. P. Oxidative DNA Damage Induced by Copper and Hydrogen Peroxide Promotes CG→TT Tandem Mutations at Methylated CpG Dinucleotides in Nucleotide Excision Repair-Deficient Cells. *Nucleic Acids Res.* **2002**, *30*, 3566–3573.
10. Stohs, S. J.; Bagchi, D. Oxidative Mechanisms in the Toxicity of Metal Ions. *Free Radical Biol. Med.* **1995**, *18*, 321–336.
11. George, S.; Xia, T.; Rallo, R.; Zhao, Y.; Ji, Z.; Lin, S.; Wang, X.; Zhang, H.; France, B.; Schoenfeld, D. Use of a High-Throughput Screening Approach Coupled with *In Vivo* Zebrafish Embryo Screening To Develop Hazard Ranking for Engineered Nanomaterials. *ACS Nano* **2011**, *5*, 1805–1817.
12. Thomas, C. R.; George, S.; Horst, A. M.; Ji, Z.; Miller, R. J.; Peralta-Videa, J. R.; Xia, T.; Pokhrel, S.; Mädler, L.; Gardea-Torresdey, J. L. Nanomaterials in the Environment: From Materials to High-Throughput Screening to Organisms. *ACS Nano* **2011**, *5*, 13–20.
13. Amatruda, J. F.; Shepard, J. L.; Stern, H. M.; Zon, L. Zebrafish as a Cancer Model System. *Cancer Cell* **2002**, *3*, 229–231.
14. Taylor, K. L.; Grant, N. J.; Temperley, N. D.; Patton, E. E. Small Molecule Screening in Zebrafish: An *In Vivo* Approach to Identifying New Chemical Tools and Drug Leads. *Cell Commun. Signal* **2010**, *8*, 11.
15. Scholz, S.; Fischer, S.; Gündel, U.; Küster, E.; Luckenbach, T.; Voelker, D. The Zebrafish Embryo Model in Environmental Risk Assessment—Applications beyond Acute Toxicity Testing. *Environ. Sci. Pollut. Res.* **2008**, *15*, 394–404.
16. Fako, V. E.; Furgeson, D. Y. Zebrafish as a Correlative and Predictive Model for Assessing Biomaterial Nanotoxicity. *Adv. Drug Delivery Rev.* **2009**, *61*, 478–486.
17. Pardo-Martin, C.; Chang, T. Y.; Koo, B. K.; Gilleland, C. L.; Wasserman, S. C.; Yanik, M. F. High-Throughput *In Vivo* Vertebrate Screening. *Nat. Methods* **2010**, *7*, 634–636.
18. Xia, T.; Zhao, Y.; Sager, T.; George, S.; Pokhrel, S.; Li, N.; Schoenfeld, D.; Meng, H.; Lin, S.; Wang, X. Decreased Dissolution of ZnO by Iron Doping Yields Nanoparticles with Reduced Toxicity in the Rodent Lung and Zebrafish Embryos. *ACS Nano* **2011**, *5*, 1223–1235.
19. Ispas, C.; Andreescu, D.; Patel, A.; Goia, D. V.; Andreescu, S.; Wallace, K. N. Toxicity and Developmental Defects of Different Sizes and Shape Nickel Nanoparticles in Zebrafish. *Environ. Sci. Technol.* **2009**, *43*, 6349–6356.
20. Asharani, P. V.; Wu, Y. L.; Gong, Z.; Valiyaveettil, S. Toxicity of Silver Nanoparticles in Zebrafish Models. *Nanotechnology* **2008**, *19*, 255102.
21. Bar-Ilan, O.; Albrecht, R. M.; Fako, V. E.; Furgeson, D. Y. Toxicity Assessments of Multisized Gold and Silver Nanoparticles in Zebrafish Embryos. *Small* **2009**, *5*, 1897–1910.
22. Asharani, P. V.; Lianwu, Y.; Gong, Z.; Valiyaveettil, S. Comparison of the Toxicity of Silver, Gold and Platinum Nanoparticles in Developing Zebrafish Embryos. *Nanotoxicology* **2011**, *5*, 43–54.
23. Yeo, M.; Kang, M. Effects of Nanometer Sized Silver Materials on Biological Toxicity during Zebrafish Embryogenesis. *Bull. Korean Chem. Soc.* **2008**, *29*, 1179–1184.
24. Wang, Y.; Seebald, J. L.; Szeto, D. P.; Irudayaraj, J. Biocompatibility and Biodistribution of Surface-Enhanced Raman Scattering Nanoprobes in Zebrafish Embryos: *In Vivo* and Multiplex Imaging. *ACS Nano* **2010**, *4*, 4039–4053.
25. Love, D. R.; Pichler, F. B.; Dodd, A.; Copp, B. R.; Greenwood, D. R. Technology for High-Throughput Screens: The Present and Future Using Zebrafish. *Curr. Opin. Biotechnol.* **2004**, *15*, 564–571.
26. Xia, T.; Kovochich, M.; Liong, M.; Mädler, L.; Gilbert, B.; Shi, H.; Yeh, J. I.; Zink, J. I.; Nel, A. E. Comparison of the Mechanism of Toxicity of Zinc Oxide and Cerium Oxide Nanoparticles based on Dissolution and Oxidative Stress Properties. *ACS Nano* **2008**, *2*, 2121–2134.
27. Ogilvie, H. C.; Mesnard, X.; Droge, J.; Wiesner, M. R. Estimating Production Data for Five Engineered Nanomaterials as a Basis for Exposure Assessment. *Environ. Sci. Technol.* **2011**, *45*, 2562–2569.
28. Burello, E.; Worth, A. P. A Theoretical Framework for Predicting the Oxidative Stress Potential of Oxide Nanoparticls. *Nanotoxicology* **2010**, *5*, 228–235.
29. Kahru, A.; Dubourguier, H. C. From Ecotoxicology to Nanoecotoxicology. *Toxicology* **2010**, *269*, 105–119.
30. King-Heiden, T. C.; Wiecinski, P. N.; Mangham, A. N.; Metz, K. M.; Nesbit, D.; Pedersen, J. A.; Hamers, R. J.; Heideman, W.; Peterson, R. E. Quantum Dot Nanotoxicity Assessment using the Zebrafish Embryo. *Environ. Sci. Technol.* **2009**, *43*, 1605–1611.
31. Bonsignorio, D.; Perego, L.; Giacco, L. D.; Cotelli, F. Structure and Macromolecular Composition of the Zebrafish Egg Chorion. *Zygote* **1996**, *4*, 101–108.
32. Rawson, D. M.; Zhang, T.; Kalicharan, D.; Jongebloed, W. L. Field Emission Scanning Electron Microscopy and Transmission Electron Microscopy Studies of the Chorion, Plasma Membrane and Syncytial Layers of the Gastrula-Stage Embryo of the Zebrafish *Brachydanio rerio*: A Consideration of The Structural and Functional Relationships with Respect to Cryoprotectant Penetration. *Aquacult. Res.* **2000**, *31*, 325–336.
33. Lee, K. J.; Nallathamby, P. D.; Browning, L. M.; Osgood, C. J.; Xu, X. H. N. *In Vivo* Imaging of Transport and Biocompatibility of Single Silver Nanoparticles in Early Development of Zebrafish Embryos. *ACS Nano* **2007**, *1*, 133–143.

34. Fent, K.; Weisbrod, C. J.; Wirth-Heller, A.; Peiles, U. Assessment of Uptake and Toxicity of Fluorescent Silica Nanoparticles in Zebrafish (*Danio rerio*) Early Life Stages. *Aquat. Toxicol.* **2010**, *2*, 218–228.
35. De Wolf, W.; Comber, M.; Douben, P.; Gimeno, S.; Holt, M.; Léonard, M.; Lillicrap, A.; Sijm, D.; Van Egmond, R.; Weisbrod, A. Animal Use Replacement, Reduction, and Refinement: Development of an Integrated Testing Strategy for Bioconcentration of Chemicals in Fish. *Integr. Environ. Assess. Manage.* **2007**, *3*, 3–17.
36. Schreiber, R.; Altenburger, R.; Paschke, A.; Schuurmann, G.; Kuster, E. A Novel *In Vitro* System for the Determination of Bioconcentration Factors and the Internal Dose in Zebrafish (*Danio rerio*) Eggs. *Chemosphere* **2009**, *77*, 928–933.
37. Zhao, J.; Bertoglio, B. A.; Devinney, M. J., Jr; Dineley, K. E.; Kay, A. R. The Interaction of Biological and Noxious Transition Metals with the Zinc Probes FluoZin-3 and Newport Green. *Anal. Biochem.* **2009**, *384*, 34–41.
38. Tõugu, V.; Karafin, A.; Palumaa, P. Binding of Zinc (II) and Copper (II) to the Full-Length Alzheimer's Amyloid-$\beta$ Peptide. *J. Neurochem.* **2008**, *104*, 1249–1259.
39. Blechinger, S. R.; Warren, J. T., Jr.; Kuwada, J. Y.; Krone, P. H. Developmental Toxicology of Cadmium in Living Embryos of a Stable Transgenic Zebrafish Line. *Environ. Health Perspect.* **2002**, *110*, 1041.
40. Blechinger, S. R.; Evans, T. G.; Tang, P. T.; Kuwada, J. Y.; Warren, J. T. The Heat-Inducible Zebrafish *hsp70* Gene Is Expressed during Normal Lens Development under Nonstress Conditions. *Mech. Dev.* **2002**, *112*, 213–215.
41. Okada, A.; Sano, K.; Nagata, K.; Yasumasu, S.; Ohtsuka, J.; Yamaura, A.; Kubota, K.; Luchi, I.; Tanokura, M. Crystal Structure of Zebrafish Hatching Enzyme 1 from the Zebrafish *Danio rerio*. *J. Mol. Biol.* **2010**, *402*, 865–878.
42. Irving, H.; Williams, R. J. P. The Stability of Transition-Metal Complexes. *J. Chem. Soc* **1953**, *637*, 3192–3210.
43. Jackson, G. S.; Murray, I.; Hosszu, L. L. P.; Gibbs, N.; Waltho, J. P.; Clarke, A. R.; Collinge, J. Location and Properties of Metal-Binding Sites on the Human Prion Protein. *Proc. Natl. Acad. Sci. U.S.A.* **2001**, *98*, 8531–8535.
44. Murata, M.; Gong, P.; Suzuki, K.; Koizumi, S. Differential Metal Response and Regulation of Human Heavy Metal-Inducible Genes. *J. Cell. Physiol.* **1999**, *180*, 105–113.
45. Santoro, M. G. Heat Shock Factors and the Control of the Stress Response. *Biochem. Pharmacol.* **2000**, *59*, 55–63.
46. Mosser, D. D.; Theodorakis, N. G.; Morimoto, R. I. Coordinate Changes in Heat Shock Element-Binding Activity and HSP70 Gene Transcription Rates in Human Cells. *Mol. Cell. Biol.* **1988**, *8*, 4736–4744.
47. Tilton, F.; Tilton, S. C.; Bammler, T. K.; Beyer, R.; Farin, F.; Stapleton, P. L.; Gallagher, E. P. Transcriptional Biomarkers and Mechanisms of Copper-Induced Olfactory Injury in Zebrafish. *Environ. Sci. Technol.* **2008**, *42*, 9404–9411.
48. Yepiskoposyan, H.; Egli, D.; Fergestad, T.; Selvaraj, A.; Treiber, C.; Multhaup, G.; Georgiev, O.; Schaffner, W. Transcriptome Response to Heavy Metal Stress in Drosophila Reveals a New Zinc Transporter That Confers Resistance to Zinc. *Nucleic Acids Res.* **2006**, *34*, 4866–4877.
49. Matz, C. J.; Krone, P. H. Cell Death, Stress-Responsive Transgene Activation, and Deficits in the Olfactory System of Larval Zebrafish following Cadmium Exposure. *Environ. Sci. Technol.* **2007**, *41*, 5143–5148.
50. Dave, G.; Xiu, R. Toxicity of Mercury, Copper, Nickel, Lead, and Cobalt to Embryos and Larvae of Zebrafish, *Brachydanio rerio*. *Arch. Environ. Contam. Toxicol.* **1991**, *21*, 126–134.
51. Griffitt, R. J.; Weil, R.; Hyndaman, K. A.; Denslow, N. D.; Powers, K.; Taylor, D.; Barber, D. S. Exposure to Copper Nanoparticles Causes Gill Injury and Acute Lethality in Zebrafish (*Danio rerio*). *Environ. Sci. Technol.* **2007**, *41*, 8178–8186.
52. Godwin, H. A.; Chopra, K.; Bradley, K. A.; Cohen, Y.; Harthorn, B. H.; Hoek, E. M. V.; Holden, P.; Keller, A. A.; Lenihan, H. S.; Nisbet, R. M. The University of California Center for the Environmental Implications of Nanotechnology. *Environ. Sci. Technol.* **2009**, *43*, 6453–6457.
53. Teoh, W. Y.; Amal, R.; Mädler, L. Flame Spray Pyrolysis: An Enabling Technology for Nanoparticles Design and Fabrication. *Nanoscale* **2010**, *2*, 1324–1347.
54. Ji, Z.; Jin, X.; George, S.; Xia, T.; Meng, H.; Wang, X.; Suarez, E.; Zhang, H.; Hoek, E. M. V.; Godwin, H. Dispersion and Stability Optimization of $TiO_2$ Nanoparticles in Cell Culture Media. *Environ. Sci. Technol.* **2010**, *44*, 7309–7314.
55. Xia, T.; Kovochich, M.; Brant, J.; Hotze, M.; Sempf, J.; Oberley, T.; Sioutas, C.; Yeh, J. I.; Wiesner, M. R.; Nel, A. E. Comparison of the Abilities of Ambient and Manufactured Nanoparticles To Induce Cellular Toxicity According to an Oxidative Stress Paradigm. *Nano Lett.* **2006**, *6*, 1794–1807.
56. Halloran, M. C.; Sato-Maeda, M.; Warren, J. T.; Su, F.; Lele, Z.; Krone, P. H.; Kuwada, J. Y.; Shoji, W. Laser-Induced Gene Expression in Specific Cells of Transgenic Zebrafish. *Development* **2000**, *127*, 1953.
57. Livak, K. J.; Schmittgen, T. D. Analysis of Relative Gene Expression Data Using Real-Time Quantitative PCR and the $2(-\Delta\Delta C(t))$ Method. *Methods* **2001**, *25*, 402–408.